THE JOURNAL OF PHYSICAL CHEMISTRY C

Subscriber access provided by READING UNIV

Article

Epitaxial Growth of Highly Oriented Metallic MoO@MoS Nanorods on C-Sapphire

Di Wu, Yingguo Yang, Peng Zhu, Xiaoming Zheng, Xiaoliu Chen, Jiao Shi, Fei Song, Xingyu Gao, Xue-Ao Zhang, Fangping Ouyang, Xiang Xiong, Yongli Gao, and Han Huang

J. Phys. Chem. C, **Just Accepted Manuscript** • DOI: 10.1021/acs.jpcc.7b10666 • Publication Date (Web): 03 Jan 2018

Downloaded from http://pubs.acs.org on January 3, 2018

Just Accepted

"Just Accepted" manuscripts have been peer-reviewed and accepted for publication. They are posted online prior to technical editing, formatting for publication and author proofing. The American Chemical Society provides "Just Accepted" as a free service to the research community to expedite the dissemination of scientific material as soon as possible after acceptance. "Just Accepted" manuscripts appear in full in PDF format accompanied by an HTML abstract. "Just Accepted" manuscripts have been fully peer reviewed, but should not be considered the official version of record. They are accessible to all readers and citable by the Digital Object Identifier (DOI®). "Just Accepted" is an optional service offered to authors. Therefore, the "Just Accepted" Web site may not include all articles that will be published in the journal. After a manuscript is technically edited and formatted, it will be removed from the "Just Accepted" Web site and published as an ASAP article. Note that technical editing may introduce minor changes to the manuscript text and/or graphics which could affect content, and all legal disclaimers and ethical guidelines that apply to the journal pertain. ACS cannot be held responsible for errors or consequences arising from the use of information contained in these "Just Accepted" manuscripts.

ACS Publications

The Journal of Physical Chemistry C is published by the American Chemical Society. 1155 Sixteenth Street N.W., Washington, DC 20036

Published by American Chemical Society. Copyright © American Chemical Society. However, no copyright claim is made to original U.S. Government works, or works produced by employees of any Commonwealth realm Crown government in the course of their duties.

Epitaxial Growth of Highly Oriented Metallic MoO_2@MoS_2 Nanorods on C-sapphire

Di Wu[1,2], Yingguo Yang[3], Peng Zhu[2], Xiaoming Zheng[1], Xiaoliu Chen[1], Jiao Shi[1], Fei Song[3], Xingyu Gao[3], Xueao Zhang[4], Fangping Ouyang[1,2], Xiang Xiong[2], Yongli Gao[1,2,5], and Han Huang[1,2,*]

[1] Hunan Key Laboratory of Super-microstructure and Ultrafast Process, School of Physics and Electronics, Central South University, Changsha 410083, P. R. China

[2] Powder Metallurgy Research Institute and State Key Laboratory of Powder Metallurgy, Central South University, Changsha 410083, P. R. China

[3] Shanghai Synchrotron Radiation Facility, Shanghai Institute of Applied Physics, Chinese Academy of Sciences, 239 Zhangheng Road, Pudong New Area, Shanghai 201204, P. R. China

[4] College of Science, National University of Defense Technology, Changsha 410073, P. R. China

[5] Department of Physics and Astronomy, University of Rochester, Rochester, NY 14627, USA

[*] Correspondence: physhh@csu.edu.cn;

Address: Hunan Key Laboratory of Super-microstructure and Ultrafast Process, School of Physics and Electronics, Central South University, No.932, South Lushan Road, Changsha City, Hunan Province, P. R. China

Abstract

Molybdenum dioxide (MoO_2) has attracted many interests due to its unique properties and potential applications. Here, we report the synthesis of high quality MoO_2@MoS_2 nanorods on c-sapphire substrates through an atmospheric pressure chemical vapor deposition (APCVD) approach. Optical microscopy (OM), cross-sectional scanning electron microscopy (SEM), high-resolution transmission electron microscopy (HRTEM), selected area electron diffraction (SAED) and (grazing incidence) X-ray diffraction ((GI)XRD) measurements reveal that these MoO_2 nanorods exhibit epitaxial growth behaviors on c-sapphire substrates with the orientation relationship of $MoO_2(100)$ || sapphire(0001) and MoO_2<001> aligned well with sapphire $<10\bar{1}0>$. Raman spectroscopy/imaging, energy dispersive spectroscopy (EDS), and GIXRD results disclose that such MoO_2 nanorods are wrapped by MoS_2 (MoO_2@MoS_2). Devices based on transferred individual MoO_2@MoS_2 nanorods show a resistivity of ~1.65×10^{-4} Ω·cm, comfirming that such nanorods possess higher crystalline degree. Our findings will be helpful for the applications of MoO_2@MoS_2 in the fields of nanoelectronic devices.

Keywords: MoO_2@MoS_2, nanorod, chemical vapor deposition, epitaxial growth, c-sapphire.

1. INTRODUCTION

Metal oxides, such as indium, zinc, molybdenum and chromium oxides, have been widely investigated due to the various outstanding properties and potential applications in electronic and photonic devices, such as gas sensors, photodetectors, supercapacitors and field-effect transistors, as well as catalysts.[1-4] For example, porous WO_3 hollow spheres have good sensitivities to alcohol, acetone, CS_2, and other organic gases.[5] As electrode for supercapacitors, MnO_2/graphene composites with needle-like nanostructures exhibit high specific capacitances and good cycling stability.[6] ZnO with complex-morphology has an enhanced performance than the vertically oriented ZnO rods when used as a catalyst for 4-chlorophenol photodecomposition.[7] The structures and compositions of $La_{1-x}Sr_xMnO_3$ are significantly changed upon annealing, which is important for spintronics and magnetic storage devices.[8] Therefore, the crystalline structures of metal oxides have significant effects on their properties.

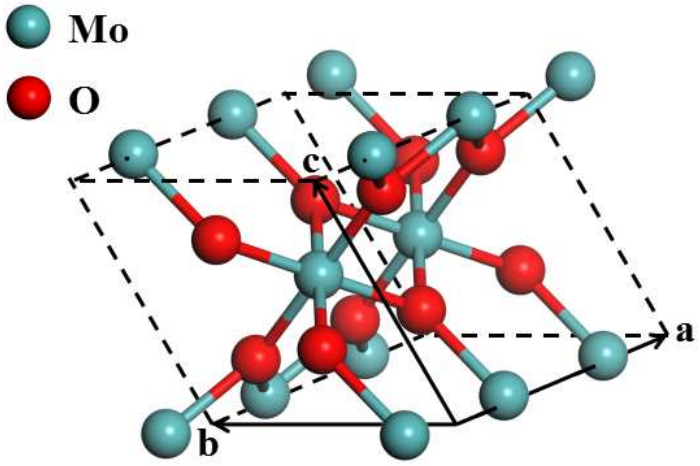

Figure 1. *Monoclinic crystal structure of MoO_2.*

Molybdenum oxides as well-known transition-metal oxides are widely applied in electronics, photodetectors, photocatalysts and organic photovoltaic devices.[9-12] In addition to a lot of

non-stoichiometric phases such as Mo_4O_{11}, Mo_9O_{26} and etc., there are two main phases: MoO_3 and MoO_2.[13,14] MoO_3 is an intrinsic n-type semiconductor with a wide bandgap (~3.2 eV) and can significantly improve the performance of organic electronics as efficient anode interfacial layers due to its high work function.[9,15] Recently, it is reported that the energy storage properties of α-MoO_3 are improved substantially by the introduction of oxygen vacancies, which is helpful for the application of MoO_3 in supercapacitors.[16] However, the low intrinsic conductivity and weak photoresponse of MoO_3 limit its applications in optoelectronic nanodevices.[17] On the contrary, MoO_2 with a monoclinic structure, as shown in Figure 1, and lattice parameters of a = 5.62 Å, b = 4.86 Å, c = 5.63 Å, and β = 120.94° is metallic and possesses a high melting point and a high chemical stability.[18-20] To date, MoO_2 with various morphologies have been successfully prepared. For example, mesoporous metallic MoO_2 thin films were synthesized by nanocasting strategy, which are usually utilized as anodes for lithium ion batteries.[21] Dispersed MoO_2 nanorods were synthesized by thermal decomposition of tetrabutylammonium hexamolybdate and vertically oriented arrays of MoO_2 nanorods were fabricated on silicon substrates by direct heating of a molybdenum spiral coil in a low vacuum.[2,22] It has been reported that metallic MoO_2 thin films (with a low resistivity of ~10^{-3} Ω·cm) can be epitaxially grown on c-sapphire through radio-frequency magnetron sputtering and pulsed laser deposition methods, because of the similar value between the height ~5.72 Å (width ~4.76 Å) of the hexagon formed by six oxygen atoms of c-sapphire surface and the lattice constants along the c-axis ~5.63 Å (b-axis ~4.86 Å) of MoO_2.[23,24] The anisotropic lattice mismatch between MoO_2(100) and sapphire(0001) may lead to anisotropic growth rates, resulting in nanorod growth.[25]

In this article, we reported the synthesis of highly oriented MoO_2@MoS_2 nanorods on c-sapphire substrates through an APCVD method. Raman spectroscopy/imaging, SEM, EDS, HRTEM, SAED

and (GI)XRD measurements were carried out. These MoO_2 nanorods are epitaxially grown on c-sapphire substrates with the orientation relationship of $MoO_2(100)$ || sapphire(0001) and MoO_2<001> in line with sapphire $<10\bar{1}0>$. Such MoO_2 nanorods are wrapped by MoS_2 due to the following sulfurization.[26] Devices based on individual MoO_2@MoS_2 nanorods are fabricated via the conventional e-beam lithography (EBL) and lift-off process and show a resistivity of ~1.65×10^{-4} Ω·cm, six fold lower than previous reports.[15,23,24] Our findings here are useful for the design of MoO_2 nanorods-based nanodevices.

2. METHODS

Experimental setup and sample characterization

The MoO_2 nanorods were synthesized by the CVD method with a two-temperature-zone system shown in Figure S1. S (Aladdin 99.999%) and MoO_3 (Aladdin 99.99%) powders were used as reductants and Mo precursors, respectively. C-sapphire and SiO_2/Si substrates were precleaned with acetone, isopropanol and hydrogen peroxide. As shown in Figure 2a, two SiO_2/Si substrates were placed with face down and the MoO_3 powder were placed under the left one. The c-sapphire substrate was supported by SiO_2/Si substrates and divided into two regions, I and II, by the quartz boat. The (0001) plane of c-sapphire faced downward. The quartz boat with MoO_3 and substrates was located at the center of the right temperature zone. The temperature of the right temperature zone raised up at a rate of 15 ℃/min to 300 ℃ under a flow rate of 300 standard-state cubic centimeter per minute (s.c.c.m.) of N_2, held at the setting temperature for 30 min, and then raised up at a rate of 13 ℃/min to 750 ℃ under a flow rate of 25 s.c.c.m., and holding for 10 min. Finally, the temperature cooled at a cooling rate of 10 ℃/min for 20 min followed by a rapid cooling under 500

s.c.c.m. of N_2. Another quartz boat containing S powders was located upstream at the center of the left temperature zone. The temperature programming for left zone was as follows: temperature held at 80 ℃ until the right zone reached a temperature of 690 ℃, and then increased with a ramping rate of 25 ℃/min to 200 ℃ and holding for 20 min followed by rapid cooling.

The OM measurements were carried out in a CaiKang DMM-200C optical microscopy. The Raman measurements were performed in a WITec alpha 300 Raman microscope using a 532 nm laser and 1800 lines/mm grating. The 520.0 cm^{-1} phonon mode from the SiO_2/Si substrate was used for calibration. Raman maps were taken at 1 mW laser power for 0.5 s with a 300 nm step size. The XRD measurements were carried out in a D/Max 2500 X-ray diffractometer with a wavelength of 0.15406 nm. The HRTEM and SAED measurements were performed in a JEOL, JEM-2100F transmission electron microscope with an acceleration voltage of 200 kV, on transferred individual nanorods. The SEM and EDS measurements on the cross-section of nanorods were performed in a Zeiss Sigma HD scanning electron microscope. Synchrotron-based GIXRD experiments were performed under ambient conditions at the BL14B1 beamline of the Shanghai Synchrotron Radiation Facility (SSRF) using X-rays with energy of 10 keV. Two dimensional GIXRD (2D-GIXRD) patterns were acquired by a MarCCD area detector mounted vertically at a distance ~230 mm from the sample.[27,28,29]

For TEM and SAED measurements, the as-grown sample was scraped using a razor blade soon after being soaked into anhydrous ethanol. The scraped ethanol containing nanorods was collected and dropped onto the TEM grid followed by air-drying for 20 min.

MoO_2 nanorods were transferred onto a SiO_2/Si substrate via the micromechanical exfoliation process using scotch tape.[30] Metal electrodes were fabricated via the conventional EBL in a RAITH

eLine Plus scanning electron microscope and electron beam deposition of Cr 10 nm and Au 100 nm, respectively. Finally, the samples were soaked in acetone for cleaning the PMMA during the lift-off process followed by ethanol rinse.

3. RESULTS AND DISCUSSION

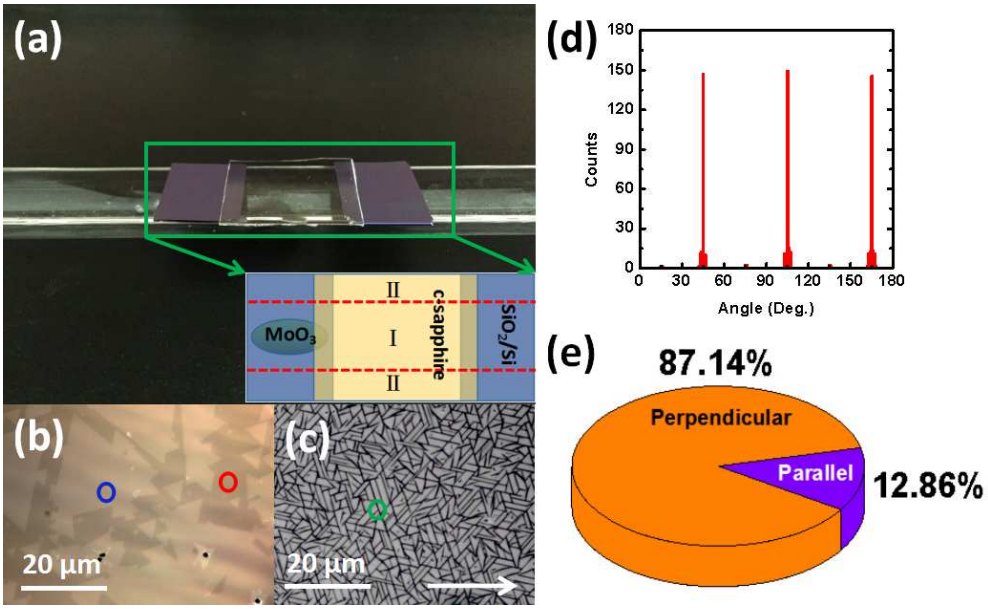

Figure 2. *(a) Photograph and corresponding schematic illustration of the position of the c-sapphire substrate relative to the MoO_3 source in the right temperature zone. The representative OM images from regions I (b) and II (c), showing the as-grown MoS_2 nanoflakes and nanorods, respectively. (d) Orientation histograms for the nanorods. The white arrow in (c) represents 0° direction. (e) The pie chart of the orientation of nanorods with respect to one edge of MoS_2 flakes.*

A typical OM image shown in Figure 2b displays that single-crystalline MoS_2 flakes in the shape of equilateral triangles are in region I, in consistence with previous reports.[31] Most of the as-grown MoS_2 flakes exhibit the same or opposite orientations, confirming the epitaxial growth mechanism.[31] In addition to a few MoS_2 flakes, many rod-like features are observed in region II, as shown in the representative OM image in Figure 2c. It can be attributed to the delivered source from the spacing between the c-sapphire and the supporting quartz boat. Most of such rods are long and straight (in the

averaged length of 20 um) and the others are short and curved. In this article, our attentions are only paid on the former nanorods which may have a relatively highly crystalline degree. The orientation histogram for such nanorods in Figure 2d shows that the growth orientations of such nanorods are centered at 45° and 45° ± 60° with respect to the horizon direction labeled by a white arrow in Figure 2c. It suggests a good epitaxial relationship of such nanorods with respect to the substrate. According to the dicing schematic of the sapphire wafer in Figure S2a, the longer border of the diced substrate is along sapphire $<10\bar{1}0>$. And Figure S2b presents a typical OM image taken close to the longer border (highlighted by a red dotted line) of the substrate, showing that the nanorods are parallel to the longer border. Thus, these nanorods grow along sapphire $<10\bar{1}0>$. It is well known that the edges of MoS_2 triangles are oriented along sapphire $<1\bar{2}10>$.[31-33] Figure 2e shows the pie chart of one edge of MoS_2 flakes with respect to the growth direction of nanorods. Among the counted 871 specimen, 87.1% (12.9%) are perpendicular (parallel) to the growth direction of nanorods, confirming above results. Randomly dispersed short rods can also be observed on the surfaces of SiO_2/Si supporters as shown in Figure S3a.

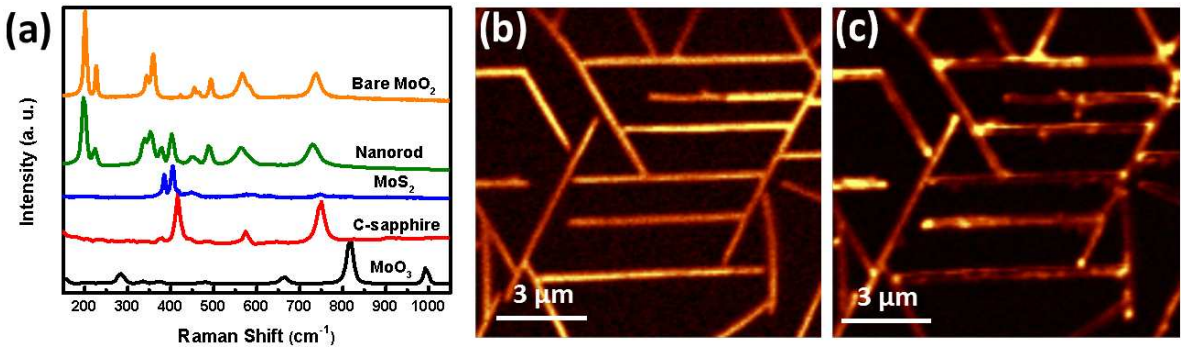

Figure 3. *(a) Raman spectra excited by 532 nm laser of bare MoO_2, nanorod, MoS_2, c-sapphire substrate and MoO_3 from the position marked by the orange, green, blue, red and black circles in Figure S4a, 2c, 2b and S4b, respectively. Raman maps of nanorods at (b) 201 and (c) 400 cm^{-1}.*

To determine the composition of such nanorods, the measurements of Raman spectroscopy were

performed. Figure 3a displays the Raman spectra (from top to bottom) of bare MoO_2 (orange solid curve), such nanorods (green solid curve), MoS_2 (blue solid curve), c-sapphire (red solid curve) and MoO_3 (black solid curve). There are two characteristic peaks for as-grown MoS_2 flakes located at ~385 and ~405 cm^{-1}, corresponding to E^1_{2g} (in-plane) and A_{1g} (out-of-plane) Raman modes respectively.[34-36] In the case of MoO_3, there are two crystalline phases: α-MoO_3 and β-MoO_3. Typical Raman peaks at 280, 660, 819, and 995 cm^{-1}, corresponding to B_{2g}, B_{3g}, B_{1g} and A_g Raman modes respectively,[37] can be observed for α-MoO_3 while two additional Raman peaks at 774 and 849 cm^{-1} can be observed for β-MoO_3.[37,38] Thus, the nanobelts in Figure S4b are α-MoO_3.[17,37] For comparison, the Raman spectrum for c-sapphire is also given, which shows three characteristic peaks at 416, 574 and 751 cm^{-1}. The Raman spectrum for the synthesized highly oriented nanorods shows several peaks at 202, 230, 344, 358, 380, 403, 452, 493, 569, 582 and 740 cm^{-1}. In addition to Raman peaks from MoS_2, it is in good agreement with that for the bare MoO_2 (orange plot in Figure 3 for the MoO_2 piece in Figure S4a.[26]) and previous report,[39-41] suggesting the main composition of these nanorods are MoO_2. It is in consistence with previous reports that MoO_3 can be reduced to form MoO_2 at high temperture.[42] The physical meanings of main Raman peaks of MoO_2 and MoO_3 are listed in Table S1.[37,38] Those at 582 and 740 cm^{-1} are attributed to the stretching vibration of the Mo-O (I) and Mo-O (II) groups in the lattice of MoO_2.[39] Considering the sulfur-rich ambience in temperature zone during the CVD reaction process at 750 ℃ with 25 s.c.c.m. N_2, the surface of such MoO_2 nanorods can be sulfurized to MoS_2, in consistence with recent reports.[43,44] The Raman spectrum of randomly dispersed short rods on SiO_2/Si substrate is similar, as shown in Figure S3b. To verify whether the chemical composition of the MoO_2 nanorods is uniform, Raman mapping measurements were conducted. Figures 3b and 3c shows Raman maps of the prepared nanorods at

201 ± 5 (MoO_2) and 400 ± 5 (MoS_2) cm^{-1}, respectively. Figure 3b presents highly oriented nanorods with uniform contrast, demonstrating the nanorods are uniform through the whole sample. While, Figure 3c shows nonuniform contrast, indicating these nanorods may be uneven sulfurized at the surface.[26] It paves the way to the useful MoO_2@MoS_2.

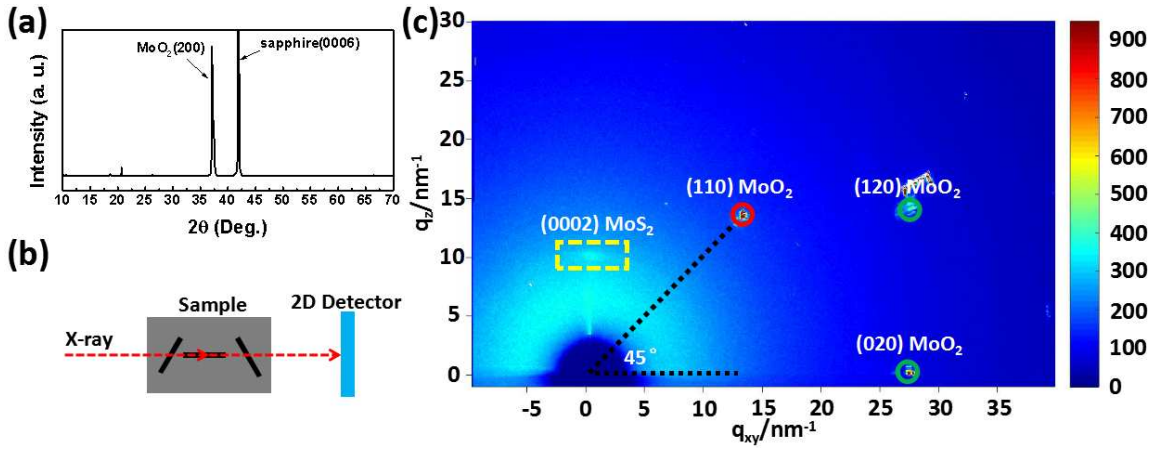

Figure 4. *(a) XRD spectrum of nanorods on c-sapphire substrate. (b) The schematic illustration of GIXRD measurements. (c) 2D-GIXRD pattern of nanorods.*

Figure 4a shows a typical XRD (θ-2θ scan) spectrum of the highly oriented nanorods on c-sapphire, which suggests a single phase. The XRD pattern displays a outstanding diffraction peak at 2θ = 37.1°, corresponding to MoO_2(200), which is similar to the results in MoO_2 films.[24,45] The sharp peak at 2θ = 41.9° corresponds to sapphire(0006).[24] It suggests that the MoO_2 nanorods are monoclinic with the orientation relationship of MoO_2(100) || sapphire(0001).[23] The diffraction peaks at 2θ =31.9°, 32.0° and 57.4° in the logarithmic scale XRD pattern in Figure S5 corresponding to MoS_2(100), (101) and (110) are much weaker,[46,47] confirming the presence of the wrapping MoS_2. The other diffraction peaks of MoO_2 may arise from the inevitable MoO_2 in other structures, such as particals and flakes as shown in Figure S4a. Figure 4b presents the schematic of GIXRD measurements. Figure 4c shows the corresponding 2D-GIXRD pattern with the incident plane of

sapphire $(1\bar{2}10)$. The diffraction maximum marked by the red circle is positioned at q_z = 13.00 nm^{-1} and q_{xy} = 12.65 nm^{-1}, which could be indexed to an interplane distance of 3.46 Å, and assigned to MoO_2(110). In addition, as shown in Figure S6, radially integrating intensity plot along the ring at q = 18.14 nm^{-1} shows that the diffraction spot concentrates at 45°, which is consistent with the dihedral angle between MoO_2(110) and MoO_2(100). As the same, the diffraction maximums marked by the green circles are assigned to MoO_2(120) and MoO_2(020). Thus, MoO_2 nanorods grow along the c-axis. All these localized sharp diffraction spots and no diffraction spots around q_{xy} = 0 (in-plane) indicate the high crystalline of the grown MoO_2 nanorods. The expended diffraction maximum positioned at q_z = 10.13 nm^{-1}, which could be indexed to an interplane distance of 6.20 Å, comes from MoS_2(0002), suggesting that MoS_2(0001) is parallel to the MoO_2(100) to form a MoO_2@MoS_2 core-shell structure. However, this value is slightly smaller than previous report,[48] which may be due to the interaction between MoO_2 and MoS_2.

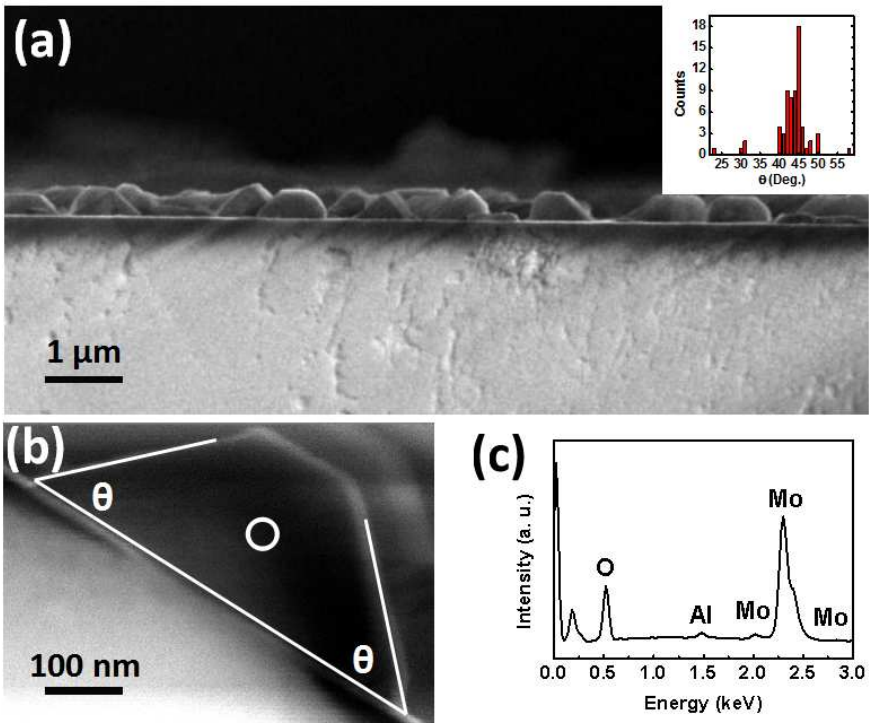

Figure 5. *(a) Cross-sectional SEM image of nanorods on c-sapphire, showing the similiar heights.*

The inset shows the angle distribution of sloping side facets of nanorods. (b) Close-up of the cross section of single nanorod. (c) EDS pattern of nanorod taken from the white circle marked area in panel (b).

Figure 5a displays a cross-sectional SEM image of a sample, showing that the cross-section of a single nanorod is in a shape either of isosceles trapezoid or of isosceles triangle. These nanorods have similar heights of about 400 nm and widths ranging from 500 to 900 nm. The cross-sectional close-up in Figure 5b displays the cross section of a single nanorod in a shape of isosceles trapezoid with a dihedral angle between sloping side facets and bottom plane of ~45°. The statistics about the angles of sloping side facets of such nanorods in the inset in Figure 5a shows that the cross sections of nanorods have base angles centered at 45°, in consistance with above GIXRD results. The existence of other base angles may be due to the sulfurization of exposed surfaces of nanorods. Thus, we conclude that the sloping side facets of nanorods are $MoO_2(110)$ and $MoO_2(1\bar{1}0)$.

Figure 5c presents the EDS spectrum taken from the position marked by white circle in Figure 5b. There are signals of three elements, corresponding to oxygen (O), aluminum (Al) and molybdenum (Mo). The signal of oxygen arises from both the c-sapphire substrate and nanorod. The signals of aluminum and molybdenum are taken from the substrate and nanorod, respectively, due to that the electron beam spot is not small enough. The atomic percentages of O, Al and Mo are 66.24%, 0.87% and 32.89%, respectively. The atomic ratio between O and Mo is calculated to be 1.97, indicating pure MoO_2 cores. However, the topographic SEM image in Figure S7a shows the existence of MoS_2. The absence of sulfur signal in the EDS in Figure S7b may be due to the atomic thickness of MoS_2. Thus, the nanorods are mainly made of single-crystalline MoO_2 and the following sulfurization from surface results in such MoO_2@MoS_2 nanorods.[26]

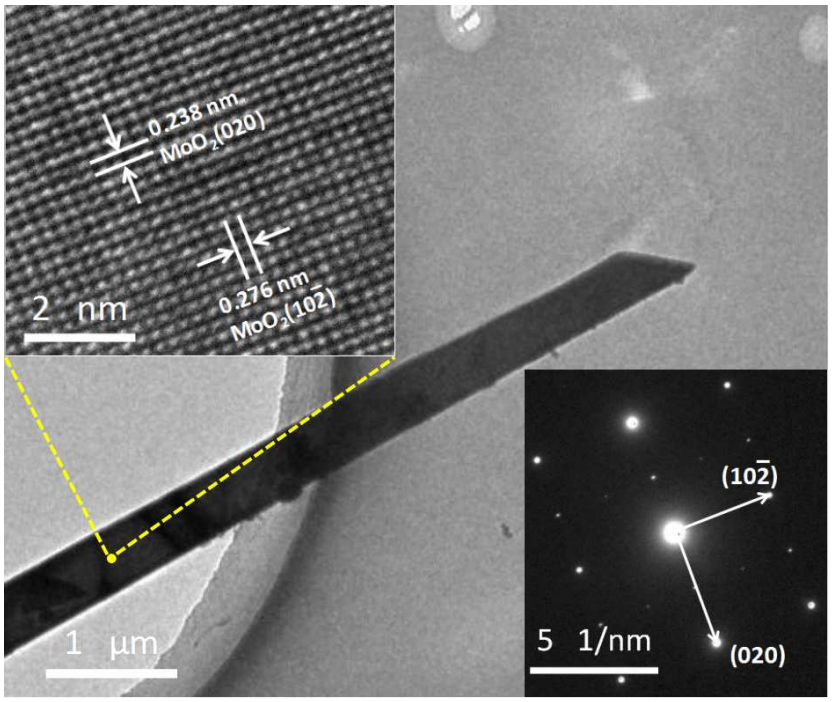

Figure 6. *Low magnification image of MoO_2 nanorod. The insets show the HRTEM image of MoO_2 nanorod in [201] zone and the corresponding SAED pattern.*

To further investigate the atomic crystal structure of these nanorods, HRTEM and SAED measurements were carried out on individual MoO_2@MoS_2 nanorods transferred onto TEM grid. Figure 6 displays a low magnification image of one MoO_2@MoS_2 nanorod, which has a similar appearance as in SEM. The corresponding SAED pattern inserted at the lower-right corner in Figure 6 with sharp diffraction spots in a two-fold symmetry indicates the two-fold symmetry of the top surface of the MoO_2 nanorod. The corresponding atomically resolved HRTEM image at the upper-left corner in Figure 6 displays the interplanar spacings of 0.238 and 0.276 nm, corresponding to the $MoO_2(020)$ and $MoO_2(10\bar{2})$, respectively. This result is consistence with the SAED pattern, confirming that these MoO_2 nanorods grow along MoO_2<001> direction. The wrapping single layered MoS_2 is transparent in TEM measurements due to the high acceleration voltage of 200 keV in our measurements and the underlying ~200 nm-thick MoO_2.[49-51]

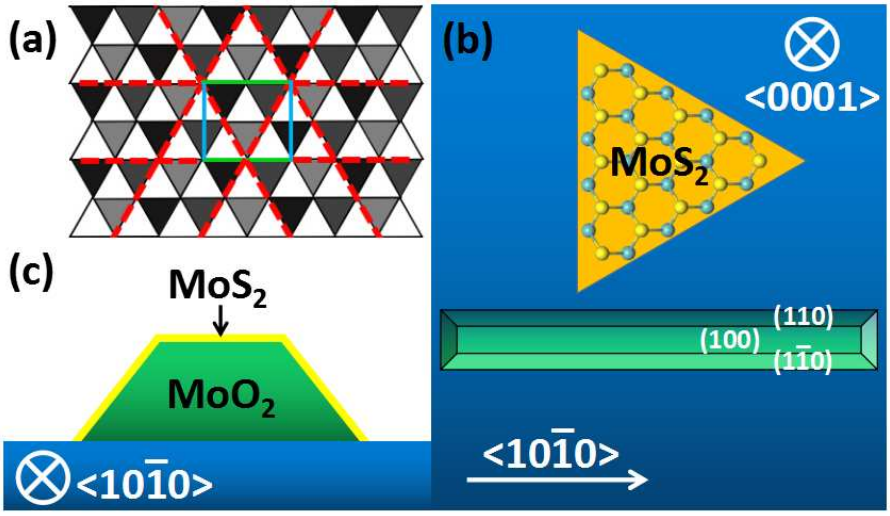

Figure 7. *(a) Schematic representation of epitaxial relationship between MoO_2(100) and c-sapphire(0001). The blue and green solid lines represent the b- and c-axis of MoO_2. The red dash lines indicate growth direction of nanorods. The junctions of the grid of triangle represent oxygen positions in the basal plane of c-sapphire. The growth schematic taken in sapphire<0001> (b) and sapphire $<10\bar{1}0>$ direction (c) of nanorods on c-sapphire substrate. The green rods represent MoO_2 nanorod, showing oriented growth along sapphire $<10\bar{1}0>$. The yellow covering on MoO_2 nanorod in (c) represents the wrapping MoS_2.*

To further demonstrate the epitaxial growth of MoO_2 nanorods on c-sapphire, a model is built. Figure 7a displays the epitaxial relationship between MoO_2(100) and sapphire(0001). The surface of c-sapphire exhibits period hexagon structure formed by oxygen atoms which are represented as the junctions of triangles with different contrasts. Each triangle indicates an octahedral hole. The bright gray, gray and dark gray triangles represent octahedral holes which are occupied by an upwardly displaced Al ion, a downwardly displaced Al ion and empty, respectively.[52] Such hexagon structure is in the height of ~5.72 Å and width of ~4.76 Å. The blue and green solid lines represent the b- and c-axis of MoO_2 nanorods (c-axis ~5.63 Å, b-axis ~4.86 Å). The anisotropic lattice mismatch, being -1.4% along the c-axis and 2.1% along the b-axis, leads to anisotropic growth rates and the growth along c-axis is faster than along b-axis.[25] Furthermore, the growth temperature in our experiments is much higher than previous,[23,24] which leads MoO_2 to more kinetic energy to overcome diffusion

barrier to grow along the c-axis. Therefore, we suggest that the formation of nanorod structure instead of film is due to the high growth temperature and anisotropic lattice mismatch between MoO_2 and c-sapphire substrate.

Figure 7b shows the growth schematic taken in sapphire<0001> direction. The blue square indicates the c-sapphire substrate. The orange triangle presents a MoS_2 flake with its edges perpendicular to sapphire $<10\bar{1}0>$. The green rod represents MoO_2 nanorod oriented along sapphire $<10\bar{1}0>$ and perpendicular to one edge of MoS_2. The top facet of MoO_2 nanorods is (100) and sloping side facets along the axial direction are (110) and $(1\bar{1}0)$. Figure 7c presents the MoO_2@MoS_2 structure taken in sapphire $<10\bar{1}0>$ direction. The yellow carpet-like feature represents the wrapping MoS_2 with MoS_2 base plane parallel to MoO_2 surfaces.

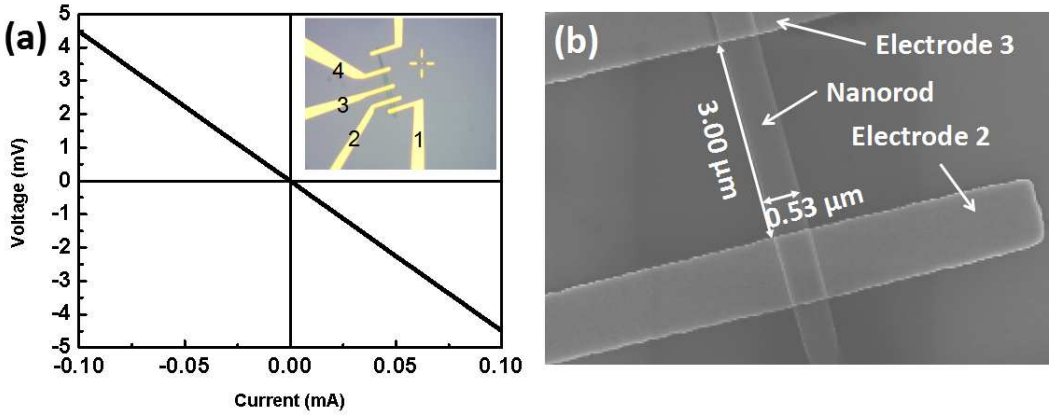

Figure 8. *(a) The V-I curve of individual nanorod. The inset the OM image of the device. (b) SEM image of the device.*

To evaluate the electrical performance of such MoO_2@MoS_2 nanorods, we introduce four-terminal method.[30] The inset in Figure 8a shows an OM image of a device. Figure 8a shows the V_{23}-I_{14} curve. Figure 8b displays the close-up SEM image of the device. The good linearity of V_{23}-I_{14} curves reveals the ohmic contact between electrodes and MoO_2@MoS_2 nanorod due to the little difference between Cr work function and MoS_2 electron affinity.[53,54] The resistivity (conductivity) of

the nanorod is calculated to be of ~1.65 × 10^{-4} Ω·m (~6.04 × 10^{3} S/cm), which is significant lower (higher) by six fold in magnitude.[24,45] Our previous temperature dependent transport measurements show the resistance of MoO_2 nanorod decreasing with the temperature decreasing.[30] It can be attributed to the epitaxial growth induced higher crystalline degree and reveals the metallic nature of the as-prepared MoO_2@MoS_2 nanorods.

4. CONCLUSION

In summary, highly oriented MoO_2@MoS_2 nanorods are synthesized on c-sapphire substrates by APCVD method and then characterized by Raman, OM, TEM, SAED, SEM, EDS and XRD measurements. Such nanorods exhibit epitaxial growth behaviors with preference for MoO_2(100) || sapphire(0001) and MoO_2<001> in line with sapphire $<10\bar{1}0>$. The anisotropic lattice mismatch and high growth temperature in our experiments lead to that MoO_2 preferentially forms nanorod structure instead of film. The sulfurization of MoO_2 nanorods from surface results in such MoO_2@MoS_2 nanorods. The higher crystalline degree of such nanorods results in a lower resistivity of ~1.65 × 10^{-4} Ω·cm. Our findings provide a method to epitaxially grow MoO_2@MoS_2 nanorods on c-sapphire with highly crystalline degree, which may be broadly applicable to other metal oxides, providing a key milestone toward fabrication of various core-shell structured materials like MoO_2@$MoTe_2$ and WO_2@WSe_2 for novel properties and functionalities. The MoO_2@MoS_2 hybrids may have great potential to be used as an active catalyst in hydrogen evolution reaction[55] and as anodes for lithium ion battery, especially at high current densities.[56]

ASSOCIATED CONTENT

Supporting Information

Figure S1, typical setup of CVD system in our experiments; Figure S2, the relationship between MoO_2@MoS_2 nanorods growth direction and sapphire $<10\bar{1}0>$; Figure S3, the OM image and Raman spectrum of MoO_2 on SiO_2/Si substrate; Table S1, The physical meanings of main Raman peaks of MoO_2 and MoO_3; Figure S4, the OM images of bare MoO_2 flake and MoO_3 nanobelt; Figure S5, XRD spectrum a logarithmic scale of MoO_2@MoS_2 nanorods; Figure S6, the radially integrating intensity of GIXRD result; Figure S7, the SEM and EDS result of MoO_2@MoS_2 nanorods.

AUTHOR INFORMATION

Corresponding author

*H. Huang. E-mail: physhh@csu.edu.cn

Notes

The authors declare no competing financial interest.

ACKNOWLEDGMENTS

We acknowledge the financial support from the National Natural Science Foundation (NSF) of China (Grants No. 11304398, 11334014, 51272291, 51173205), the NSF of Hunan province (Grants No. 2015JJ1020, 2016JJ1021) and the Innovation-Driven project of Central South University (Grants No. 2015CXS1035, 2017CX018). Prof. Y. Gao acknowledges the support from National Science Foundation (DMR-1303742, CBET-1437656). Dr. D. Wu acknowledges the support from the Fundamental Research Funds for the Central Universities of Central South University (Grants No.

2015zzts160, 2017zzts330).

REFERENCES:

(1) Huang, M. H.; Mao, S.; Feick, H.; Yan, H. Q.; Wu, Y. Y.; Kind, H.; Weber, E.; Russo, R.; Yang, P. D. Room-Temperature Ultraviolet Nanowire Nanolasers. *Science* **2001**, *292***,** 1897.

(2) Rajeswari, J.; Kishore, P. S.; Viswanathan, B.; Varadarajan, T. K. One-Dimensional MoO_2 Nanorods for Supercapacitor Applications. *Electrochem. Commun.* **2009**, *11*, 572.

(3) Wan, Q.; Dattoli, E.; Lu, W. Doping-Dependent Electrical Characteristics of SnO_2 Nanowires. *Small* **2008**, *4*, 451-454.

(4) Li, Y. G.; Tan, B.; Wu, Y. Y. Mesoporous Co_3O_4 Nanowire Arrays for Lithium Ion Batteries with High Capacity and Rate Capability. *Nano Lett.* **2008**, *8*, 265-270.

(5) Li, X. L.; Lou, T. J.; Sun, X. M.; Li, Y. D. Highly Sensitive WO_3 Hollow-Sphere Gas Sensors. *Inorg. Chem*. **2004**, *43*, 5442-5449.

(6) Mao, L.; Zhang, K.; Chan, H. S. O.; Wu, J. S. Nanostructured MnO_2/Graphene Composites for Supercapacitor Electrodes: The Effect of Morphology, Crystallinity and Composition. *J. Mater. Chem*. **2012**, *22*, 1845-1851.

(7) Tian, Z. R. R.; Voigt, J. A.; Liu, J.; McKenzie, B.; McDermott, M. J.; Rodriguez, M. A.; Konishi, H.; Xu, H. F. Complex and Oriented ZnO Nanostructures. *Nat. Mater*. **2003**, *2*, 821-826.

(8) Xie, H. P.; Huang, H.; Cao, N. T.; Zhou, C. H.; Niu, D. M.; Gao, Y. L. Effects of Annealing on Structure and Composition of LSMO Thin Films. *Physica B* **2015**, *477*, 14-19.

(9) Kyaw, A. K. K.; Sun, X. W.; Jiang, C. Y.; Lo, G. Q.; Zhao, D. W.; Kwong, D. L. An Inverted Organic Solar Cell Employing A Sol-Gel Derived ZnO Electron Selective Layer and Thermal Evaporated MoO_3 Hole Selective Layer. *Appl. Phys. Lett*. **2008**, *93*, 221107.

(10) Papp, J.; Soled, S.; Dwight, K.; Wold, A. Surface Acidity and Photocatalytic Activity of TiO_2, WO_3/TiO_2, and MoO_3/TiO_2 Photocatalysts. *Chem. Mater*. **1994**, *6*, 496-500.

(11) Song, K. Y.; Park, M. K.; Kwon, Y. T.; Lee, H. W.; Chung, W. J.; Lee, W. I. Preparation of Transparent Particulate MoO_3/TiO_2 and WO_3/TiO_2 Films and Their Photocatalytic Properties. *Chem. Mater*. **2001**, *13*, 2349-2355.

(12) Liu, P.; Liu, X. L.; Lyu, L.; Xie, H. P.; Zhang, H.; Niu, D. M.; Huang, H.; Bi, C.; Xiao, Z. G.; Huang, J. S.; et al. Interfacial Electronic Structure at The $CH_3NH_3PbI_3$/MoO_x Interface. *Appl. Phys. Lett*. **2015**, *106*, 193903.

(13) Canadell, E.; Whangbo, M. H.; Schlenke, Cr.; Escribe-Filippini, C. Band Electronic Structure Study of The Electronic Instability in The Magneli Phase Molybdenum Oxide [Mo_4O_{11}]. *Inorg. Chem.* **1989**, *28*, 1466.

(14) Ekström, T.; Tilley, R. J. D. Ternary Tungsten Oxides with The Mo_5O_{14} Structure. *Journal of Solid State Chemistry* **1976**, *19*, 125.

(15) Xiang, D.; Han, C.; Zhang, J. L.; Chen, W. Gap States Assisted MoO_3 Nanobelt Photodetector with Wide Spectrum Response. *Sci. Rep.* **2014**, *4*, 4891.

(16) Kim, H. S.; Cook, J. B.; Lin, H.; Ko, J. S.; Tolbert, S. H.; Ozolins, V.; Dunn, B. Oxygen Vacancies Enhance Pseudocapacitive Charge Storage Properties of MoO_{3-x}. *Nat. Mater.* **2017**, *16*, 454.

(17) Balendhran, S.; Deng, J. K.; Ou, J. Z.; Walia, S.; Scott, J.; Tang, J. S.; Wang, K. L.; Field, M. R.; Russo, S.; Zhuiykov, S.; et al. Enhanced Charge Carrier Mobility in Two-Dimensional High Dielectric Molybdenum Oxide. *Adv. Mater*. **2013**, *25*, 109-114.
(18) Fang, X. P.; Guo, B. K.; Shi, Y. F.; Li, B.; Hua, C. X.; Yao, C. H.; Zhang, Y. C.; Hu, Y. S.; Wang, Z. X.; Stucky, G. D.; et al. Enhanced Li Storage Performance of Ordered Mesoporous MoO_2 via Tungsten Doping. *Nanoscale* **2012**, *4*, 1541-1544.
(19) Yang, L. J.; Zhou, W. J.; Hou, D. M.; Zhou, K.; Li, G. Q.; Tang, Z. H.; Li, L. G.; Chen, S. W. Porous Metallic MoO_2-Supported MoS_2 Nanosheets for Enhanced Electrocatalytic Activity in The Hydrogen Evolution Reaction. *Nanoscale* **2015**, *7*, 5203-5208.
(20) Brandt, B. G.; Skapski, A. C. A Refinement of The Crystal Structure of Molybdenum Dioxide. *Acta Chem. Scand*. **1967**, *21*, 661-672.
(21) Shi, Y. F.; Guo, B. K.; Corr, S. A.; Shi, Q. H.; Hu, Y. S.; Heier, K. R.; Chen, L. Q.; Seshadri, R.; Stucky, G. D. Ordered Mesoporous Metallic MoO_2 Materials with Highly Reversible Lithium Storage Capacity. *Nano Lett*. **2009**, *9*, 4215-4220.
(22) Liu, J. G.; Zhang, Z. J.; Pan, C. Y.; Zhao, Y.; Su, X.; Zhou, Y.; Yu, D. P. Enhanced Field Emission Properties of MoO_2 Nanorods with Controllable Shape and Orientation. *Mater. Lett*. **2004**, *58*, 3812-3815.
(23) Ahn, E.; Seo, Y. S.; Cho, J.; Lee, I.; Hwang, J.; Jeen, H. Epitaxial Growth and Metallicity of Rutile MoO_2 Thin Film. *RSC Adv*. **2016**, *6*, 60704.
(24) Bhosle, V.; Tiwari, A.; Narayan, J. Epitaxial Growth and Properties of MoO_x ($2< x< 2.75$) Films. *J. Appl. Phys*. **2005**, *97*, 083539.
(25) Singh, A.; Jansen, C.; Lahabi, K.; Aarts, J. High-Quality CrO_2 Nanowires for Dissipation-less Spintronics. *Phys. Rev. X* **2016**, *6*, 041012.
(26) Wang, X. S.; Feng, H. B.; Wu, Y. M.; Jiao, L. Y. Controlled Synthesis of Highly Crystalline MoS_2 Flakes by Chemical Vapor Deposition. *J. Am. Chem. Soc.* **2013**, *135*, 5304-5307.
(27) Feng, S. L.; Yang, Y. G.; Li, M.; Wang, J. M.; Cheng, Z. D.; Li, J. H.; Ji, G. W.; Yin, G. Z.; Song, F.; Wang, Z. K.; et al. High-Performance Perovskite Solar Cells Engineered by An Ammonia Modified Graphene Oxide Interfacial Layer. *ACS Appl. Mater. Interfaces* **2016**, *8*, 14503-14512.
(28) Yang, Y. G.; Feng, S. L.; Li, M.; Wu, Z. W.; Fang, X.; Wang, F.; Geng, D. P.; Yang, T. Y.; Li, X. L.; Sun, B. Q.; et al. Structure, Optical Absorption, and Performance of Organic Solar Cells Improved by Gold Nanoparticles in Buffer Layers. *ACS Appl. Mater. Interfaces* **2015**, *7*, 24430-24437.
(29) Yang, Y. G.; Feng, S. L.; Xu, W. D.; Li, M.; Li, L.; Zhang, X. M.; Ji, G. W.; Zhang, X. N.; Wang, Z. K.; Xiong, Y. M.; et al. Enhanced Crystalline Phase Purity of $CH_3NH_3PbI_{3-x}Cl_x$ Film for High-Efficiency Hysteresis-Free Perovskite Solar Cells. *ACS Appl. Mater. Interfaces* **2017**, *9*, 23141-23151.
(30) Xie, Q. L.; Zheng, X. M.; Wu, D.; Chen, X. L.; Shi, J.; Han, X. T.; Zhang, X. A.; Peng, G.; Gao, Y. L.; Huang, H. High Electrical Conductivity of Individual Epitaxially Grown MoO_2 Nanorods. *Appl. Phys. Lett*. **2017**, *111*, 093505.
(31) Dumcenco, D.; Ovchinnikov, D.; Marinov, K.; Lazic, P.; Gibertini, M.; Marzari, N.; Sanchez, O. L.; Kung, Y. C.; Krasnozhon, D.; Chen, M. W.; et al. Large-Area Epitaxial Monolayer MoS_2. *ACS Nano* **2015**, *9*, 4611-4620.
(32) Chen, Y.; Bagnall, D. M.; Koh, H. J.; Park, K. T.; Hiraga, K.; Zhu, Z.; Yao, T. Plasma Assisted Molecular Beam Epitaxy of ZnO on c-Plane Sapphire: Growth and Characterization. *J. Appl. Phys*.

1998, *84*, 3912-3918.
(33) Ouyang, F. P.; Yang, Z. X.; Ni, X.; Wu, N. N.; Chen, Y.; Xiong, X. Hydrogenation-Induced Edge Magnetization in Armchair MoS_2 Nanoribbon and Electric Field Effects. *Appl. Phys. Lett*. **2014**, *104*, 071901.
(34) Scheuschner, N.; Gillen, R.; Staiger, M.; Maultzsch, J. Interlayer Resonant Raman Modes in Few-Layer MoS_2. *Phys. Rev. B* **2015**, *91*, 235409.
(35) Wang, S. S.; Rong, Y. M.; Fan, Y.; Pacios, M.; Bhaskaran, H.; He, K.; Warner, J. H. Shape Evolution of Monolayer MoS_2 Crystals Grown by Chemical Vapor Deposition. *Chem. Mater*. **2014**, *26*, 6371–6379.
(36) Wu, D.; Huang, H.; Zhu, X. P.; He, Y. W.; Xie, Q. L.; Chen, X. L.; Zheng, X. M.; Duan, H. G.; Gao, Y. L. E" Raman Mode in Thermal Strain-Fractured CVD-MoS_2. *Crystals* **2016**, *6*, 151.
(37) Camacho-Lopez, M. A.; Escobar-Alarcon, L.; Picquart. M.; Arroyo, R.; Cordoba. G. Micro-Raman Study of The m-MoO_2 to α-MoO_3 Transformation Induced by cw-Laser Irradiation. *Opt. Mater*. **2011**, *33*, 480-484.
(38) Haro-Poniatowski, E.; Julien, C.; Pecquenard, B.; Livage, J.; Camacho-López, M. A. Laser-Induced Structural Transformations in MoO_3 Investigated by Raman Spectroscopy. *J. Mater. Res*. **1998**, *13*, 1033-1037.
(39) Kumari, L.; Ma, Y. R.; Tsai, C. C.; Lin, Y. W.; Wu, S. Y.; Cheng, K. W.; Liou, Y. X-ray Diffraction and Raman Scattering Studies on Large-Area Array and Nanobranched Structure of 1D MoO_2 Nanorods. *Nanotechnology* **2007**, *18*, 115717.
(40) Spevack, A.; Mctintyre, N. S. Thermal Reduction of Molybdenum Trioxide. *J. Phys. Chem.* **1992**, *96*, 9029.
(41) Dieterle, M.; Mestl, G. Raman Spectroscopy of Molybdenum Oxides Part I. Structural Characterization of Oxygen Defects in MoO_{3-x} by DR UV/VIS, Raman Spectroscopy and X-ray Diffraction. *Phys. Chem. Chem. Phys*. **2002**, *4*, 822-826.
(42) Wan, W.; Li, H.; Huang, H.; Wong, S. L.; Lv, L.; Gao, Y. L.; Wee, A. T. S. Incorporating Isolated Molybdenum (Mo) Atoms into Bilayer Epitaxial Graphene on 4H-SiC(0001). *ACS Nano*, **2013**, *8*, 970-976.
(43) Park, T.; Leem, M.; Lee, H.; Ahn, W.; Kim, H.; Kim, J.; Lee, E.; Kim, Y. H.; Kim, H. Synthesis of Vertical MoO_2/MoS_2 Core-Shell Structures on an Amorphous Substrate via Chemical Vapor Deposition. *J. Phys. Chem. C* **2017**, DOI: 10.1021/acs.jpcc.7b08171.
(44) DeGregorio, Z. P.; Yoo, Y.; Johns, J. E. Aligned MoO_2/MoS_2 and MoO_2/$MoTe_2$ Freestanding Core/Shell Nanoplates Driven by Surface Interactions. *J. Phys. Chem. Lett.* **2017**, *8*, 1631–1636
(45) Hu, B.; Mai, L. Q.; Chen, W.; Yang, F. From MoO_3 Nanobelts to MoO_2 Nanorods: Structure Transformation and Electrical Transport. *ACS Nano* **2009**, *3*, 478-482.
(46) Hao, S.; Yang, B. C.; Gao, Y. L. Chemical Vapor Deposition Growth and Characterization of Drop-Like MoS_2/MoO_2 Granular Films. *Phys. Status Solidi B*, **2017**, *254*, 1600245.
(47) Lee, Y. H.; Zhang, X. Q.; Zhang, W. J.; Chang, M. T.; Lin, C. T.; Chang, K. D.; Yu, Y. C.; Wang, J. T. W.; Chang, C. S.; Li, L. J.; et al. Synthesis of Large-Area MoS_2 Atomic Layers with Chemical Vapor Deposition. *Adv. Mat*. **2012**, *24*, 2320-2325.
(48) Zhang, L.; Yang, Y. G.; Huang, H.; Lyu. L.; Zhang, H.; Cao, N. T.; Xie, H. P.; Gao, X. Y.; Niu, D. M.; Gao, Y. L. Thickness-Dependent Air-Exposure-Induced Phase Transition of CuPc Ultrathin Films to Well-Ordered One-Dimensional Nanocrystals on Layered Substrates. *J. Phys. Chem. C* **2015**, *119*, 4217-4223.

(49) Kumar, P.; Singh, M.; Sharma, R. K.; Reddy, G. B. A Study on Role of Partial Pressure in Controlled Synthesis of Core-shell MoO_2/MoS_2 Nanoflakes. *Mater. Chem. Phys.* **2016**, 178, 6-11.
(50) van der Zande, A. M.; Huang, P. Y.; Chenet, D. A.; Berkelbach, T. C.; You, Y. M.; Lee, G. H.; Heinz, T. F.; Reichman, D. R.; Muller, D. A.; Hone, J. C. Grains and Grain Boundaries in Highly Crystalline Monolayer Molybdenum Disulphide. *Nat. Mater*. **2013**, *12*, 554-561.
(51) Li, M. Y.; Shi, Y. M.; Cheng, C. C.; Lu, L. S.; Lin, Y. C.; Tang, H. L.; Tsai, M. L.; Chu, C. W.; Wei, K. H.; He, J. H.; et al. Epitaxial Growth of a Monolayer WSe_2-MoS_2 Lateral p-n Junction with an Atomically Sharp Interface. *Science* **2015**, *349*, 524-528.
(52) Zhang, K. H. L.; Lazarov, V. K.; Galindo, P. L.; Oropeza, F. E.; Payne, D. J.; Lai, H. H. C.; Egdell, R. G. Domain Matching Epitaxial Grouth of In_2O_3 Thin Films on α-Al_2O_3(0001). *Cryst. Growth Des*. **2012**, *12*, 1000-1007.
(53) Radisavljevic, B.; Radenovic, A.; Brivio, J.; Giacometti, V.; Kis, A. Single-layer MoS_2 Transistors. *Nat. Nanotech*. **2011**, *6*, 147-150.
(54) Kim, C.; Moon, I.; Lee, D.; Choi, M. S.; Ahmed, F.; Nam, S.; Cho, Y.; Shin, H. J.; Park, S.; Yoo, W. J. Fermi Level Pinning at Electrical Metal Contacts of Monolayer Molybdenum Dichalcogenides. *ACS Nano* **2017**, *11*, 1588-1596.
(55) Nikam, R. D.; Lu, A. Y.; Sonawane, P. A.; Kumar, U. R.; Yadav, K.; Li, L. J.; Chen, Y. T. Three-Dimensional Heterostructures of MoS_2 Nanosheets on Conducting MoO_2 as An Efficient Electrocatalyst to Enhance Hydrogen Evolution Reaction. *ACS Appl. Mater. Interfaces* **2015**, *7*, 23328-23335.
(56) Xiao, D. B.; Zhang, J. Y.; Li, X.; Zhao. D.; Huang, H. Y.; Huang, J. L.; Cao, D. X.; Li, Z. H.; Niu, C. M. Nanocarved MoS_2-MoO_2 Hybrids Fabricated Using in Situ Grown MoS_2 as Nanomasks. *ACS Nano* **2016**, *10*, 9509-9515.

TABLE OF CONTENTS (TOC)